La Metallurgia Italiana
International Journal of the Italian Association for Metallurgy

DOI 10.36146/2026_03_45

The effect of continuous casting conditions on the mechanical properties of low-carbon steel wire rods

F. Baldussi, A. Chugaeva, A. Milan, A. Parimbelli, F. Guerra, L. Angelini, M. G. Gelfi, A. Pola

Solidification plays a fundamental role in metallurgical processes, such as continuous casting of steel billets, as it greatly influences the final microstructure, in terms of chemical segregation, grains morphology and size. Segregation of solute elements occurs because of their partitioning between the liquid and the growing solid. The liquid interdendritic regions are enriched of solute elements rejected by the growing dendrites. Such segregation cannot be fully mitigated through subsequent hot rolling processes. Common evidence of this undesirable phenomenon is the banded microstructure observed in hot-rolled products, characterized by alternating longitudinal bands of ferrite and pearlite. Normalization can reduce the banded microstructure, but micro-segregation remains difficult to completely homogenize. Therefore, hot-rolled wire rods produced from steel billets solidified under different conditions exhibit varying mechanical properties. In this context, the study presents a comparative analysis of two low-carbon steel billets with similar chemical composition but produced under different casting conditions with two different casting machines. The analysis investigated the differences in macro and micro-structure of the two billets by measuring the secondary dendrite arm spacing (SDAS) and the segregation index. The mechanical properties of wire rods derived from the billets were assessed by tensile tests and micro-hardness Vickers measurements. The microstructures (of billets and wire rods) were analyzed by optical and scanning electron microscopy (SEM) equipped with an energy dispersive spectrometer (EDS).

KEYWORDS: STEEL, CONTINUOUS CASTING, SOLIDIFICATION STRUCTURE, SDAS, MECHANICAL PROPERTIES;

INTRODUCTION

The steel wire used to produce screws and bolts is commonly obtained by continuous casting of billets that are hot rolled, transformed into wire rods, and finally cold worked. Continuous casting is the predominant process in steel production because of its high efficiency, quality, and automation compared to traditional ingot casting [1, 2]. As well known, the typical billet solidification structure obtained by this process, when observing a cross section, is composed of three different regions: a surface equiaxed grain zone, a columnar zone, and a central equiaxed zone. The surface zone, also called chill zone, consists of a layer of fine equiaxed grains, formed from the molten steel in contact with the cooled copper mold. In fact, the highly undercooled liquid and its convective movement are responsible for the fine and dense number of grains. Beneath this layer columnar grains grow along

Federico Baldussi, Marcello Giuseppe Gelfi, Annalisa Pola
Dipartimento di Ingegneria Meccanica e Industriale, Università degli Studi di Brescia, Brescia, Italy

Angelina Chugaeva, Alessandro Milan, Francesco Guerra, Lorenzo Angelini, Andrea Parimbelli
Acciaierie di Calvisano S.p.A., Feralpi Group, Italy

the heat exchange direction, driven by the heat extraction towards the mold. At the core, equiaxed grains nucleated in the highly constitutionally supercooled molten metal and by small pieces of the columnar grains broken by the relative movement between liquid and already solidified phases [3]. Due to the lower cooling rate in this area, the resulting equiaxed grains are coarser than those in the chill zone. Solidification structure and its quality are of great importance, as they influence the final properties of steel product [4]. The use of electromagnetic stirrers during continuous casting also affects the cast product properties. In particular, the magnetic field is able to alter dendrite arm spacing, grain size [5], columnar to equiaxed transition [6, 7], and to homogenize the chemical composition, reducing the central segregation and the solidification interface morphology [8]. However, when the stirring effect is too strong, a white band can be observed in the cast billet, corresponding to a negative segregation region at the solidification interface [9]. As previously mentioned, the solidification of the continuously cast billets, occurs in the dendritic mode [4]. Therefore, the growing dendrites reject dissolved elements in the nearby liquid, due to the different solubility of elements in the solid and liquid phases [10]. Partitioning of rejected solute elements is responsible for both micro and macro segregation that, with the solidification structure, affects the final product quality and properties. Such chemical segregations, formed during solidification of the billet, cannot be removed during the subsequent reheating and hot rolling process [11]. In fact, a banded microstructure, formed by longitudinal alternating bands of ferrite and pearlite, is the common result of the micro-segregation of alloying elements in the hot rolled products, which reduces the mechanical properties of the final component, and can be mitigated only after a normalizing heat treatment [12]. The rolling process aligns the chemical variations in the interdendritic regions, producing bands with low and high concentrations of solute elements [3]. Since solidification conditions affect dendritic growth and the consequent elements partitioning, which causes segregations, secondary dendrite arm spacing (SDAS) could be used as an indicator of the interdendritic segregation. Moreover, since the SDAS is also influenced by the heat transfer during solidification, it gives information about the solidification rate, increasing with decreasing cooling rate [3]. In summary, because the solidification structure that forms under a certain set of casting parameters affects the mechanical properties of the final hot rolled product [4, 13, 14], it follows the need of a precise control of the entire production process to fulfill the final product quality.

In this research, a comparative analysis was performed on 27MnB4 mod C + Si + Mn steel billets, produced by two different steelmaking plants. The two billets, named A and B, were hot rolled to produce wire rods of different diameters in the same plant with the constant parameters. However, an evident difference in the mechanical properties of the final wire rods was observed, consistently, for every diameter produced. Therefore, the solidification structure and segregation of the billets were evaluated and compared, along with the microstructure and mechanical properties of the final products. The results were then related to the two different continuous casting processes.

MATERIALS AND METHODS

The analysis was focused on two 27MnB4 mod C + Si + Mn steel grade. Two billets (A and B) were produced, both 8000 mm long with a cross section of approximately 160 mm x 160 mm. Billet A was produced in a casting machine with a curvature radius of about 5 meters equipped with mold electromagnetic stirrers (MEMS) and strand electromagnetic stirrers (SEMS). Billet B was produced in a machine without SEMS, with a curvature radius of about 8 meters. The specific secondary cooling used for billet B was less intense than for billet A, but the cooling was distributed along a longer region of the strand. Subsequently, billets A and B were hot rolled in the same plant with the same process parameters.

Hence, both billets (with chemical composition shown in table 1) were sectioned to obtain sections about 20 mm thick. Two sections, one from billet A and one from billet B, were etched with diluted sulfuric acid (15% H_2SO_4, 85% H_2O) for 10 hours and then macroscopically inspected, according to the UNI 3138 standard.

Tab.1 - Chemical composition of A and B steel billets.

STEEL COMPOSITION															
Billet	**C%**	**Mn%**	**Si%**	**P%**	**S%**	**Cu%**	**Cr%**	**Ni%**	**Mo%**	**Sn%**	**Al%**	**Ti%**	**N%**	**B%**	**Ceq**
A	0.26	0.90	0.13	0.010	0.002	0.18	0.11	0.10	0.02	0.008	0.024	0.047	0.0087	0.0035	0.454
B	0.26	0.87	0.13	0.011	0.004	0.18	0.17	0.09	0.03	0.009	0.021	0.041	0.0126	0.0030	0.465

The sections not selected for macroscopic inspection were cut into four parts (see figure 1a). Three of these parts (called Slice 1, Slice 3 and Slice 4) were then further divided into four parts to obtain smaller samples, to facilitate handling during the subsequent metallographic preparation and analysis. The two samples of the Slices 1 (1.1, 1.2) containing the half diagonal of the billets, after grinding and polishing, were etched using Nital 2% for 10 seconds. Using an optical microscope (Leica DMI 5000M) the microstructure was evaluated in the four regions specified in figure 1a (i.e.: a: external zone; b: ¼ external diagonal; d: ¼ internal diagonal; c: core), and some micrographs were collected for each of the specified zones. The four observed zones (a, b, c, d) were about 10 mm in diameter. The average ferritic grain dimension in these four regions was evaluated using an optical microscope (Leica DM4 M) at 100x magnification, equipped with LAS X software, in accordance with the Intercept method presented in ASTM E112. To verify the results, the measurements were repeated also applying the Comparison method for average grain size determination, as described in the same standard.

The pieces of Slice 4 (4.1, 4.2) were used to determine the prior austenite grain size (PAGS) in the four regions already described for the slice n° 1(a, b, c, d). The PAGS was assessed by using the Khon method to reveal the austenitic grains, as prescribed by UNI EN ISO 643:2024 standard, applying the Comparison method for the measurements.

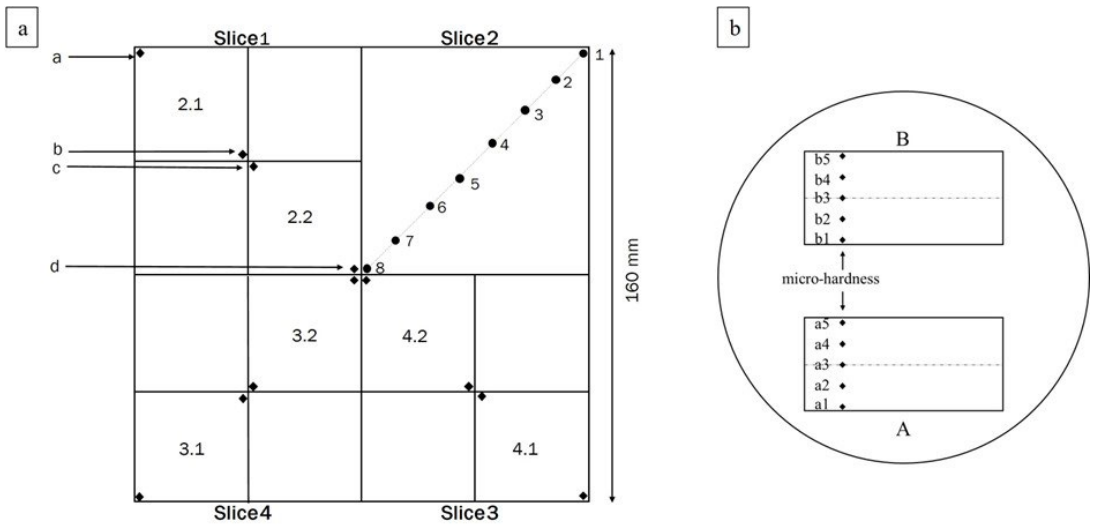

Fig.1 - Scheme of sample collection, a) billets samples, b) wire rods samples.

The two samples of Slices 3 (3.1, 3.2), along the diagonal of the billet were heat treated as presented by Wang et al. [15] to highlight the original solidification structure. In particular, the specimens were heated to 930°C at 10°C/min and held for 30 minutes, then cooled to 680°C at 5°C/min and held for 120 minutes, followed by cooling to room temperature in the furnace. The specimens were ground, polished, etched with Nital 4% for 5

seconds. A macrograph was collected for each specimen to visually observe the evolution of the solidification structure and to better identify the columnar to equiaxed transition. The specimens were also observed under an optical microscope at 50x magnification to evaluate the SDAS values in the four selected regions. At least twenty dendrites were measured per zone. Method C, as presented by Vandersluis et al. [16], was used to determine the SDAS.

Finally, Slices 2 were designated for chemical analysis. The carbon and sulfur contents of eight different positions along the slice's diagonal were measured, as shown in figure 1a. Samples were drilled by using a 5 mm diameter drill to a depth of 8mm. The chips were analyzed using an elemental analyzer (Eltra CS2000). The C and S trends along the billet were evaluated, and carbon segregation indexes were determined dividing the local carbon content by the average value, as suggested by Lan et al. [17]

$$S_i = {}^{C_i}/_{C_{mean}} \qquad [1]$$

where S_i is the segregation index at the measured position, C_i is the local carbon content, and C_{mean} is the average carbon content of the eight analyzed regions.

The wire rods produced from the two steel billets were also examined. For mechanical properties, wire rods of various diameters were tested, while for the microstructural analysis, two wire rods with 7.5 mm diameter (one from wire rod A, and one from wire rod B) were selected. A longitudinal cross section (7.5 mm x 20.0 mm) was taken from each wire rod for microscopic examination. The two small samples were mounted in a general-purpose thermosetting resin (figure 1b). The samples were then ground, mirror polished and etched with Nital 2%: the sample from wire rod A for 20 seconds, and the sample from wire rod B for 15 seconds. For each sample, Vickers microhardness measurements were taken at five different positions (as illustrated in figure 1b) by using a load of 1 kg. Position (a and b) 1 and 5 were near the specimen surfaces, at a distance of at least 2.5 times the diagonal length of the hardness indentation. Measurements (a and b) 2 and 4 were made halfway between the surface and the longitudinal axis (1.875 mm from the surface), and position (a and b) 3 was located along the longitudinal axis (3.75 mm from the sides). Each measurement was repeated three times per sample. Microstructural analysis was performed at the same five positions, using the hardness indentation as a reference, to determine the ferritic grain size in precise positions. The micrographs were collected at a 100x magnification using an optical microscope (Leica DM4 M) equipped with LAS X software, at a sufficient distance from the hardness indentation to avoid any influence. The ferritic grain size was evaluated in the five zones, in accordance with the Intercept method described in ASTM E112 and verifying the results repeating the measurement applying the Comparison method presented in the same standard.

The banded microstructure of the two wire rods was also investigated by SEM-EDS analysis, using a Leo Evo 40XVP scanning electron microscope equipped with an Oxford energy-dispersive X-ray spectrometer. Chemical evaluation of the Mn and C content were conducted along a path from the surface to the longitudinal axis, to detect localized segregation. For greater accuracy, the chemical composition of the ferrite and perlite bands were also analyzed.

Two additional samples were taken from each wire rod and polished to mirror finishing for non-metallic inclusion analysis. The inclusion count was performed by optical microscope while the Zeiss Sigma 360 scanning electron microscope equipped with the EDS microanalysis was used to determine their chemical composition.

RESULTS AND DISCUSSION

The macroscopic examinations of the two billet slices revealed the first difference.

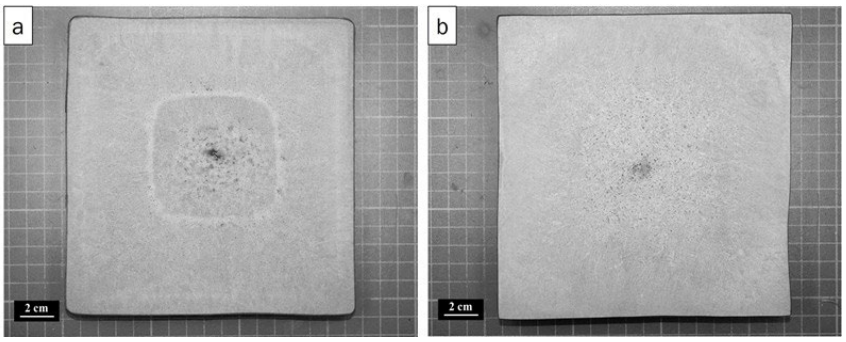

Fig.2 - Macrograph of A and B billets sections etched with sulfuric acid. a) billet A section, b) billet B section.

Billet A (figure 2a), produced using SEMS, shows the white band, a characteristic negative segregation, often visible in the cross section of billets produced by using strand electromagnetic stirrers. The band corresponds to the solid-liquid interface when stirring occurs [9, 18]. The white band has a diameter of approximately 72 mm. Billet B, produced without SEMS, does not show this peculiar feature (figure 2b).

The white band in billet A can also be seen in the macrograph of the 3.2 piece (figure 3a). From the macrographs of the four samples heat-treated and etched with Nital 4% (pieces 3.1 and 3.2 for A and B billets; figure 3), the extent of the equiaxed and columnar zones is clearly visible. For billet A, the columnar to equiaxed transition occurs at approximately one quarter of the billet diagonal (figure 3a).

The equiaxed region accounts for 32% of the total billet cross section area. The white band is entirely located within the equiaxed region (figure 3b). Therefore, the SEMS acts on the liquid steel after the columnar to equiaxed transition has occurred, helping to homogenize the chemical composition and temperature gradient of the molten steel at the core of the billet, thereby reducing the centerline defects. Billet B presents a more extended columnar region; the transition to the equiaxed structure is delayed and occurs closer to the billet core (figure 3d). In fact, the equiaxed zone accounts for only 14% of the billet cross section area, which is less than half of that of billet A. The larger columnar region in billet B could be due to a higher superheat of the steel and a high cooling rate, particularly in the initial primary cooling zone, in the mould region.

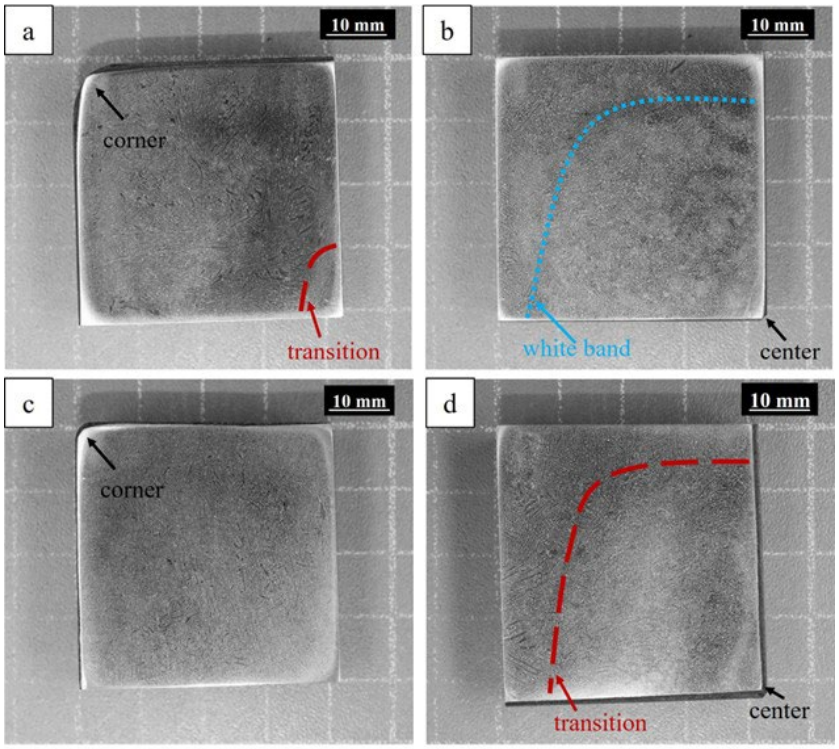

Fig.3 - Macrograph of A and B billets samples heat treated and etched with Nital. a) A 3.1 sample, b) A 3.2 sample, c) B 3.1 sample, d) B 3.2 sample.

Billet A PAGS presents a G value of about 7.5 while billet B a G value of 7.0. The microstructure of both A and B billets (figure 4) consists of ferrite and pearlite, as expected for this C-Mn steel. Both steels present a microstructure that becomes coarser moving from the surface to the core of the billet, due to decreasing cooling rate. Billet A (figure 4a) shows finer grains compared to B billet (figure 4b), with an average grain size of 26.9 μm. Billet B has an average grain size of 31.9 μm, which is about 18% larger than that of billet A. This difference may be due to the higher secondary cooling rate used for billet A, which was stronger and concentrated over a shorter length. In contrast, for billet B it was longer and divided into more subregions; thus, despite the initial intensive cooling in the mould region, it then becomes milder in the secondary cooling zones. As a result, billet A exits the secondary cooling region at lower temperature. Hence, the billet A remains at high temperature for a shorter time, preventing the coarsening of the γ grains, and promoting the formation of smaller ferritic-pearlitic grains compared to billet B during the subsequent transformation at lower temperature.

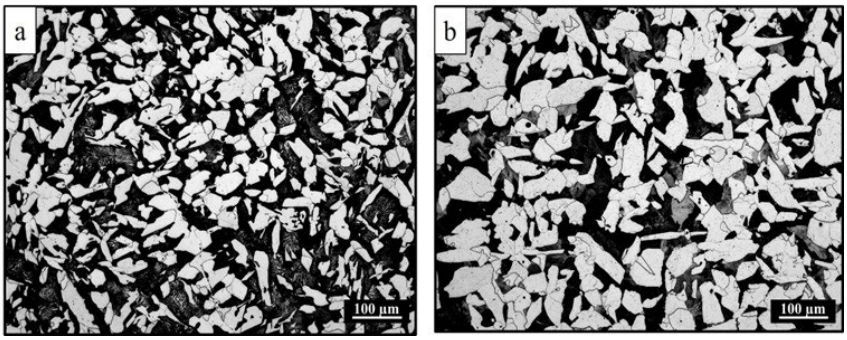

Fig.4 - Billets microstructure, a) billet A, b) billet B.

Figure 5a shows the SDAS values determined for the samples (Slice 3) in the four selected zones, for both billets. As can be seen, in both cases the SDAS values grow moving from the external zone to the core of the billets.

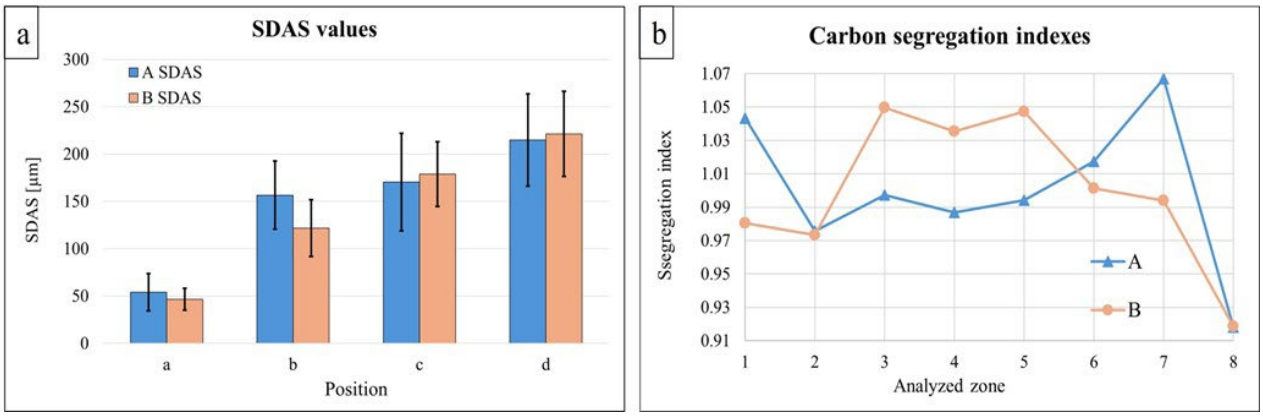

Fig.5 - a) SDAS values for A and B billets in the four selected regions; b) Carbon segregation index measured in different positions of billets A and B cross-sections.

For billet A, the small SDAS value measured in the external zone (figure 5a) shows an abrupt increase moving toward the core, because of the rapid transition from columnar to equiaxial growth that was detected in b position of the 3.1 sample. The billet A maximum SDAS value is 215 ±49 μm, at the core of the billet. In billet B, the SDAS growth (figure 5a) from the external position to the core is more gradual, due to the larger extension of the columnar zone. The SDAS values at b and c positions for billet B are different despite their proximity because, during the

columnar growth, the solidification rate decreases moving towards the center of the billet. In the equiaxial zone at the core of the billet, instead, the solidification is more homogeneous and occurs almost simultaneously in the liquid mass, with slight differences between nearby areas. Billet A and B have comparable SDAS values in the four analyzed zone. The only notable difference is observed at position B, where billet A exhibits a slightly higher SDAS value due to the presence of an already developed equiaxed solidification structure, while billet B still shows a predominantly columnar solidification morphology at the same location.

Carbon and sulfur contents for the two billets (A and B), were measured on the diagonal of Slice 2 (figure 1a) with the elemental analyzer Eltra CS2000. Billet B presents a higher sulfur average content (32.7 ppm) respect to billet A (13.2 ppm). The difference is almost constant in the eight positions analyzed along the billet's diagonal, confirming the chemical composition presented in table 1. Looking at carbon content, billet B has an average value of about 0,25 ±0.011 %, while billet A presents a higher value of about 0,26 ± 0.012 %. The segregation index measured in the selected positions of the two samples is presented in the figure 5b. The difference in C content is not sufficient to affect markedly the material mechanical properties. Billet A shows larger segregation indexes respect to billet B in the internal zones, near the billet core, with a maximum value of about 1,07. The SEMS acts near position 5 in billet A (white band is close to this position). The billet A segregation indexes in the position 1 to 6 are homogeneous. On the contrary, in regions 7 and 8, which are the last that solidify and far from the SEMS influence zone, the segregation indexes exhibit a variable trend.

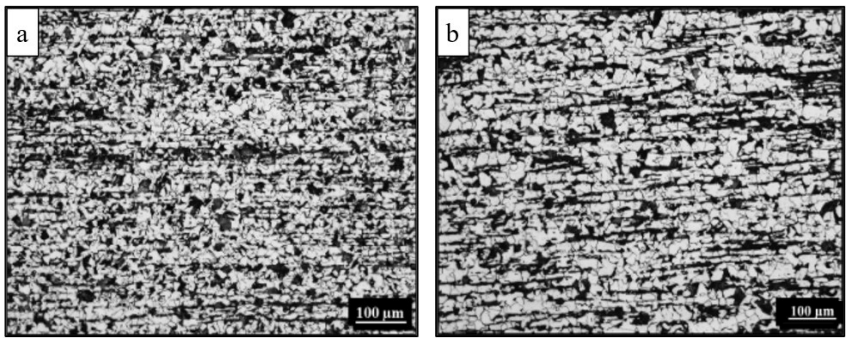

Fig.6 - Wire rods microstructure, a) wire rod A, b) wire rod B.

In figure 6, the microstructure of the wire rods manufactured from billed A and B are reported. The wire rod B shows marked bands of ferrite and pearlite (figure 6b), especially in the core zone of the sample, along the longitudinal axis. Moreover, the wire rod A presents a finer microstructure (figure 6a) with an average ferritic grain size of 6.1 µm, while the B wire rod average grain size is 8.4 µm, that is 39% larger than the wire rod A sample. The larger grain size for the wire rod B is responsible for the marked banded microstructure, as larger grains form bigger bands. It is worth noting that the microstructure of billet B is coarser than that of billet A. Therefore, after the hot rolling process, wire rod B microstructure is also expected to be coarser than that of wire rod A, given that the hot rolling process parameters are the same for both billets. A larger equiaxed region, a comparable SDAS, and a finer microstructure of the billet, lead to a finer microstructure in the wire rod, after the hot rolling process [19].

The mechanical properties of the two wire rods A and B (table 2) are consistent with the observed difference in grain size. Wire rod A, with the finer microstructure, has also higher properties, with yield strength and tensile strength exceeding those of wire B by as much as 23 MPa.

Tab.2 - Yield strength, tensile strength and area reduction at fracture of A and B wire rods.

MECHANICAL PROPERTIES			
Wire rod	**σy [MPa]**	**σr [MPa]**	**Z%**
A	381 ± 33	592 ± 32	66 ± 2
B	358 ± 19	569 ± 26	66 ± 3

Considering the Hall-Petch relation, it is possible to predict the effects of grain size on the yield strength of metals through the formula:

$$\sigma_y = \sigma_i + k_y d^{-1/2} \qquad [2]$$

where σ_y is the yield strength, σ_i is the overall resistance of the lattice to dislocation movement; ky is the grain boundary locking term which measures the relative hardening contribution by the grain boundaries, and d is the grain diameter [20]. For low carbon steel, a k_y value of 15 $MN/m^2mm^{1/2}$ can be assumed [21], resulting in a difference in yield strength between the two sample of 29 MPa. This value is quite in agreement with the difference measured by tensile tests (i.e. 23 MPa). Vickers micro-hardnesses also confirm the difference in the mechanical properties. As expected, also in this case, the finer microstructure of wire rod A is responsible for a superior hardness value. Wire rod A presents a hardness average value of 179 ± 4 HV, while wire rod B has an average value of 160 ± 5 HV. Using the conversion table provided in the ASTM A370-15 standard to compare the hardness value to the tensile strength, the measured σ_r difference is confirmed.

The SEM-EDS analysis performed to assess the segregation of Mn or C along the banded microstructure from the surface to the core of the wire rod samples revealed no significant difference between the two wire rods samples, indicating that no remarkable segregation is present. This confirms the chemical analysis on the two billets, where no significant segregation was detected. Comparable results were obtained also for the chemical analysis of pearlite and ferrite and for the non-metallic inclusion count.

CONCLUSIONS

The observed discrepancy in the mechanical properties of the wire rods produced from the two steel billets can be attributed to the different microstructures resulting from their respective solidification conditions. Billet A, which underwent a higher cooling rate during solidification, developed a finer microstructure and a significantly larger equiaxed zone, approximately twice as wide as that of billet B, while maintaining a comparable SDAS. These initial features contributed to the formation of a finer microstructure in the hot-rolled wire rod. As mechanical properties are significantly influenced by grain size, the finer microstructure of wire rod A results in enhanced yield and tensile strength in comparison to wire rod B despite similar values of area reduction.

ACKNOWLEDGEMENTS

The authors would like to thank the laboratories staff of MetalL@BS (Università degli Studi di Brescia), and the staff of the quality department of Acciaierie di Calvisano S.p.A.* and Arlenico S.p.A.* (*Feralpi Group).

REFERENCES

[1] Y. Nian et al., "Application Status and Development Trend of Continuous Casting Reduction Technology: A Review," Processes, vol. 10, p. 2669, 12/12 2022, doi: 10.3390/pr10122669.

[2] A. Vakhrushev et al., "Electric Current Distribution During Electromagnetic Braking in Continuous Casting," Metallurgical and Materials Transactions B, vol. 51, pp. 1-18, 09/01 2020, doi: 10.1007/s11663-020-01952-3.

[3] G. Krauss, "Solidification, segregation, and banding in carbon and alloy steels," Metallurgical and Materials Transactions B, vol. 34, no. 6, pp. 781-792, 2003/12/01 2003, doi: 10.1007/s11663-003-0084-z.

[4] Y. Ji, H. Tang, P. Lan, C. Shang, J. Zhang, "Effect of Dendritic Morphology and Central Segregation of Billet Castings on the Microstructure and Mechanical Property of Hot-Rolled Wire Rods," Steel Research International, vol. 88, p. 1600426, 02/01 2017, doi: 10.1002/srin.201600426.

[5] J. Kovács, A. Rónaföldi, Á. Kovács, A. Roósz, "Effect of the rotating magnetic field on the unidirectionally solidified macrostructure of Al6Si4Cu alloy," Transactions of the Indian Institute of Metals, vol. 62, no. 4, pp. 461-464, 2009/10/01 2009, doi: 10.1007/s12666-009-0085-y.

[6] S. Eckert, B. Willers, P. A. Nikrityuk, K. Eckert, U. Michel, G. Zouhar, "Application of a rotating magnetic field during directional solidification of Pb–Sn alloys: Consequences on the CET," Materials Science and Engineering: A, vol. 413-414, pp. 211-216, 2005/12/15/ 2005, doi: https://doi.org/10.1016/j.msea.2005.09.014.

[7] T. Sun, F. Yue, H.-J. Wu, C. Guo, Y. Li, Z.-C. Ma, "Solidification structure of continuous casting large round billets under mold electromagnetic stirring," Journal of Iron and Steel Research International, vol. 23, no. 4, pp. 329-337, 2016/04/01 2016, doi: 10.1016/S1006-706X(16)30053-X.

[8] X. Li, Y. Fautrelle, Z. Ren, "Influence of thermoelectric effects on the solid-liquid interface shape and cellular morphology in the mushy zone during the directional solidification of Al-Cu alloys under a magnetic field," Acta Materialia, vol. 55, no. 11, pp. 3803-3813, 2007/06/01/ 2007, doi: https://doi.org/10.1016/j.actamat.2007.02.031.

[9] C. Yao et al., "Effects of Secondary Cooling Segment Electromagnetic Stirring on Solidification Behavior and Composition Distribution in High-Strength Steel 22MnB5," JOM, Article vol. 74, no. 12, pp. 4823-4830, 2022, doi: 10.1007/s11837-022-05542-3.

[10] X. Zhang, C. Xu, C. Lei, T. Wang, H. Lin, H. Wu, "Study on Stirring Effect of Spiral Magnetic Field in Continuous Casting of Round Blooms," steel research international, vol. 95, no. 1, p. 2300278, 2024/01/01 2024, doi: https://doi.org/10.1002/srin.202300278.

[11] H. Preßlinger, M. Mayr, E. Tragl, C. Bernhard, "Assessment of the Primary Structure of Slabs and the Influence on Hot- and Cold-Rolled Strip Structure," Steel Research International, vol. 77, pp. 107-115, 02/01 2006, doi: 10.1002/srin.200606362.

[12] W. A. Spitzig, "Effect of sulfide inclusion morphology and pearlite banding on anisotropy of mechanical properties in normalized C-Mn steels," Metallurgical Transactions A, vol. 14, no. 1, pp. 271-283, 1983/02/01 1983, doi: 10.1007/BF02651624.

[13] X. Li, X. Wang, Y. Bao, J. Gong, W. Pang, M. Wang, "Effect of Electromagnetic Stirring on the Solidification Behavior of High-Magnetic-Induction Grain-Oriented Silicon Steel Continuous Casting Slab," JOM, vol. 72, 02/11 2020, doi: 10.1007/s11837-020-04058-y.

[14] C. Yao et al., "Effect of traveling-wave magnetic field on dendrite growth of high-strength steel slab: Industrial trials and numerical simulation," International Journal of Minerals, Metallurgy and Materials, vol. 30, no. 9, pp. 1716-1728, 2023/09/01 2023, doi: 10.1007/s12613-023-2629-2.

[15] H. Wang et al., "Dendrite Structure, Spot Segregation and Banded Defect of Gear Steel in Continuous Casting and Rolling Process," Metallurgical and Materials Transactions B, vol. 54, no. 2, pp. 895-912, 2023/04/01 2023, doi: 10.1007/s11663-023-02734-3.

[16] E. Vandersluis and C. Ravindran, "Comparison of Measurement Methods for Secondary Dendrite Arm Spacing," Metallography, Microstructure, and Analysis, vol. 6, no. 1, pp. 89-94, 2017/02/01 2017, doi: 10.1007/s13632-016-0331-8.

[17] P. Lan, C. Su, H. Ai, "Solidification Structure and Segregation in Billet Continuous Casting Under High Casting Speed for Alloyed Steel," Metallurgical and Materials Transactions B: Process Metallurgy and Materials Processing Science, Article vol. 55, no. 6, pp. 5093-5109, 2024, doi: 10.1007/s11663-024-03314-9.

[18] M. R. Bridge, G. D. Rogers, "Structural effects and band segregate formation during the electromagnetic stirring of strand-cast steel," Metallurgical Transactions B, vol. 15, no. 3, pp. 581-589, 1984/09/01 1984, doi: 10.1007/BF02657390.

[19] S. S. Raza et al., "Effect of hot rolling on microstructures and mechanical properties of Ni base superalloy," Vacuum, vol. 174, p. 109204, 2020/04/01/ 2020, doi: https://doi.org/10.1016/j.vacuum.2020.109204.

[20] R. Lumley, A. Morton, I. Polmear, "Nanoengineering of metallic materials," in Nanostructure Control of Materials, R. H. J. Hannink and A. J. Hill Eds.: Woodhead Publishing, 2006, pp. 219-250. doi:10.1533/9781845691189.219

[21] M.-Y. Seok, I.-C. Choi, J. Moon, S. Kim, U. Ramamurty, J.-I. Jang, "Estimation of the Hall-Petch strengthening coefficient of steels through nanoindentation," Scripta Materialia, vol. 87, pp. 49-52, 2014/09/15/ 2014, doi: https://doi.org/10.1016/j.scriptamat.2014.05.004.

TORNA ALL'INDICE >